Results in Surfaces and Interfaces 17 (2024) 100291

Contents lists available at ScienceDirect

Results in Surfaces and Interfaces

journal homepage: www.elsevier.com/locate/rsurfi

Ethanol properties effects on its reaction with Mo-doped SnO_2 clusters: A gas sensor model

Mudar Ahmed Abdulsattar [a,*], Rashid Hashim Jabbar [a], Mohammed A. Al-Seady [b,c]

[a] Ministry of Science and Technology, Baghdad, Iraq
[b] Department of Theoretical Physics, University of Szeged, Tisza Lajos Krt. 84-86, Szeged, 6720, Hungary
[c] Environmental Research and Studies Center, University of Babylon, Babylon, Iraq

ARTICLE INFO

Keywords:
Mo-doping
SnO_2 cluster
Ethanol gas sensor
Density functional theory
Transition state

ABSTRACT

The reaction of ethanol with pristine and Mo-doped SnO_2 is computed and compared to experimental results. The comparison includes response, response time, and the effect of humidity. Adsorption and transition states are evaluated and used to calculate the reaction rate of ethanol with pristine and Mo-doped SnO_2. The modified Evans–Polanyi principle is used to evaluate Gibbs free energy of transition, including its components enthalpy and entropy at the investigated doping percentages of Mo at 3, 5, and 7 mol%. The effect of humidity on the backward reaction of ethanol burning is discussed. The impact of the autoignition temperature of ethanol at 368 °C on the reaction rate is included for the first time for Mo-doped SnO_2. The theoretical results show good agreement with the experiment. Mo-doped SnO_2 shows high response, short response time, and stability towards ethanol that nominate the sensor for practical applications.

1. Introduction

Chemical sensors are one of the most used sensors in addition to other sensors such as biochemical and image sensors. SnO_2 is one of a group of metal oxides that are frequently used in sensing many gases such as NH_3 (Zhu et al., 2024), ethanol (Xu et al., 2024), NO_2 (Ding et al., 2024), etc. SnO_2 is also an oxygen-deficient n-type semiconductor (Sahu and Das, 2018). Other oxides include ZnO (Bonyani et al., 2024), WO_3 (Yang et al., 2024), Fe_2O_3 (Pan et al., 2024) etc. SnO_2 has the privilege over other metal oxides by the number of oxygen vacancies that enhance the detection process (Wang et al., 2021). Doping (Nzaba et al., 2024) is a method that can increase gas sensitivity to higher levels. The most efficient dopants in gas sensors are the Pt group (such as Pd, Ru, and Rh) (Chen et al., 2022) or other noble transition metals (such as Au, Ag, and Hg) (Hsu et al., 2020). However, because of their high price, the Pt group or other noble transition metals are replaced by other cheaper elements such as Fe (Vaishampayan et al., 2008), Mo (Wang et al., 2021), and Ni (Manikandan et al., 2020). These elements can enhance gas sensing by different mechanisms. For example, MoO_3 is a p-type semiconductor (Manikandan et al., 2020) forming a p-n junction with SnO_2 on doping. The higher oxidation state of Mo (6) adds more oxygen to the already existing in SnO_2. The detection limit of doped SnO_2 can reach small values of the detected gas, such as 1 ppm (Wang et al., 2021).

Ethanol (C_2H_6O) is a necessary industrial material precursor to many other materials (van Dyk et al., 2024). Ethanol's properties, such as its ability to dissolve many different materials, are also crucial in the industry (Afifah et al., 2024). Being drinkable alcohol also provides additional reasons to detect ethanol in addition to its other industrial applications. Properties such as autoignition temperature (368 °C) are essential in both applications and detection of ethanol (Chen et al., 2010). In applications, ethanol temperature should not approach autoignition temperature to avoid ethanol explosion. In detection, ethanol cannot be detected in temperatures near autoignition temperature since it has already burned or exploded before reaching these temperatures. Autoignition temperature is a good indicator for distinguishing between gases (Redd et al., 2024). As an example, the autoignition temperature of ethanol (368 °C) can be distinguished easily from that of H_2 (536 °C) (Hydrogen autoignition temperature) or acetone (465 °C) (Material Safety Data Sheet) etc. As a result, a gas detected in a temperature higher than 368 °C should not be ethanol.

Modeling gas sensors is a complicated process since the properties of both the sensor surface and detected gas (and the combination) must be modeled to obtain the final detection process modeling. Density

* Corresponding author.
E-mail address: mudarahmed3@yahoo.com (M.A. Abdulsattar).

https://doi.org/10.1016/j.rsurfi.2024.100291
Received 31 July 2024; Received in revised form 29 August 2024; Accepted 3 September 2024
Available online 5 September 2024

functional theory (DFT) is usually the appropriate tool for this process (Nguyet et al., 2024; Mafa et al., 2023). Reaction and adsorption theories are commonly used to model gas sensors. First, the detected gas is physisorbed (physisorption due to van der Waals forces) on the surface of the sensor. The physisorption process changes the conductivity of the sensor very weakly in most cases. The second step is the chemisorption or reaction of the gas with the sensing material. The reaction step changes the sensor's conductivity much higher than the physisorption process. For example, CO_2 gas is detected weakly compared to CO gas since CO_2 gas mainly experiences only physisorption while CO reacts with the sensor's surface (Araújo et al., 2023).

Reaction theories are modeled in many methods. One of the first reaction theories is the Arrhenius equation (He et al., 2024). However, a more recent formalism is available in the transition state theory (Abdulsattar et al., 2024). Variations and modifications of these reaction theories are widely distributed among corresponding scientific applications. Usually, the temperature and concentration dependence of the investigated reaction are of great importance (Malefane et al., 2020).

The present work investigates the sensitivity of pristine and Mo-doped SnO_2 surface clusters to ethanol. Transition state theory is applied to model the present gas sensor application. Thermodynamic quantities such as Gibbs free energy, enthalpy, and entropy are calculated to manifest the temperature dependence of the sensing operation. The modified Evans–Polanyi principle is used to interpolate the values of Gibbs free energy of transition for the different Mo doping percentages. Theoretical results are compared with available experimental results. No previous DFT calculations for ethanol sensitivity by Mo-doped SnO_2 exist in the literature, nor do they exist for the effect of ethanol gas properties on Mo-doped SnO_2.

2. Theory

Gaussian 09 computational software is used to evaluate the present study's results. The B3LYP version of DFT is combined with a basis set 6-311G**. Dispersion correction (GD3BJ) is added since it is essential for gas sensor calculations (Abdulsattar, 2023a). The B3LYP/6-311G** combination proved successful in gas sensor calculations (Abdulsattar, 2020). The B3LYP level is usually the most successful DFT version in many applications, combined with 6-311G** basis and dispersion corrections, ensuring long-range interactions are included in calculations. The accuracy of the DFT method used is also controlled by the time needed to execute structural optimizing computational routines. Of course, using more sophisticated basis sets will need longer structural optimization time that can go beyond the capabilities of our computational facilities.

SnO_2 surface pyramids are known to cover the SnO_2 surface (Jagadish et al., 2022). These pyramids are responsible for the interaction with outer space gases (Abdulsattar and Mahmood, 2023). These pyramids are oxygen deficient ($Sn_{10}O_{16}$), as can be seen from the formula of the SnO_2 pyramid shown in Fig. (1a). The stability of the SnO_2 pyramid towards the reaction with oxygen can be investigated via Gibbs free energy of the reaction. Removing or adding oxygen atoms to the $Sn_{10}O_{16}$ cluster ends with a positive Gibbs free energy that means it is unfavorable (Abdulsattar, 2020). The same is true for Mo-doped SnO_2 cluster. The most stable Mo-doped SnO_2 cluster is $MoSn_9O_{17}$ which is a result of replacing an Sn atom by Mo atom in the $Sn_{10}O_{16}$ cluster (Fig. 1b). The stability of this cluster can be tested by the following equations:

$$MoSn_9O_{17} \rightarrow MoSn_9O_{16} + \tfrac{1}{2}O_2 \ (\Delta G = 3.452 \text{ eV}), \quad (1)$$

$$MoSn_9O_{17} + \tfrac{1}{2}O_2 \rightarrow MoSn_9O_{18} \ (\Delta G = 0.897 \text{ eV}). \quad (2)$$

As can be seen from the above two equations, the $MoSn_9O_{17}$ cluster cannot give or accept oxygen atoms from the atmosphere because of the positive value of Gibbs free energy of the reaction. The extra oxygen atom in $MoSn_9O_{17}$ is because Mo oxidation state is (+6) higher than Sn (+4). The surface pyramids grow on SnO_2 tetragonal structure (Thirumoorthi and Prakash, 2016). The Sn–O is calculated to be 2.11 Å compared to the experimental 2.06 Å (Chen et al., 2023).

The reaction rate theories are usually temperature-andconcentration-dependent. The transition state theory is one of the most frequently used theories (Shefer et al., 2022) to calculate reaction rates. The general form of this theory applied to the present reaction of SnO_2 with ethanol can be given by (Knopf and Ammann, 2021):

$$\frac{d[SnO2]}{dt} = -[SnO2]^u [C_2H_6O]_e^v k(T), \quad (1)$$

$$k(T) = A\ T^m \exp\left(\frac{-\Delta G^{\ddagger}}{k_B T}\right). \quad (2)$$

In the above equations, $[SnO_2]$ and $[C_2H_6O]$ represent the concentration of SnO_2 and ethanol, respectively. The concentration exponents (u and v) in Eq. (1) are determined experimentally and usually take the values 1 or ½. The value of u is always equal to 1 in literature (Abdulsattar et al., 2024), while the value of v will be discussed in the results section. The subscript (e) in the ethanol concentration refers to the effective concentration of ethanol. Ethanol burns out in the atmospheric oxygen as it approaches its autoignition temperature at 368 °C (Chen et al., 2010), which reduces concentration as the sensor approaches autoignition temperature. The preexponential constant (A) in

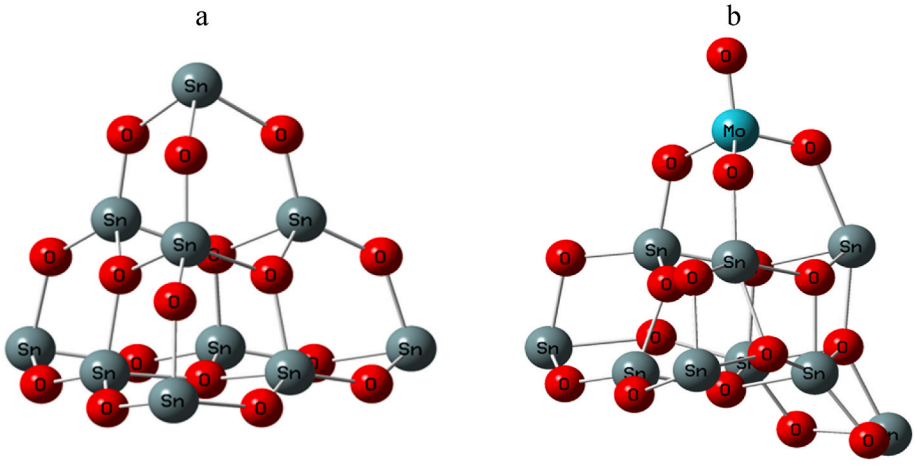

Fig. 1. Shows (a) The optimized structure of SnO_2 clusters ($Sn_{10}O_{16}$) and (b) the optimized $MoSn_9O_{17}$ molecule. Every atom is assigned by its symbol: O for oxygen, Sn for tin, and Mo for molybdenum.

Eq. (2) depends on the sensor material properties' structure, morphology, crystallinity, surface area, doping, etc. The temperature exponent (m) determines the steepness of the reaction rate increase as temperature increases. $\Delta G^{\ddagger}$ is Gibbs free energy of transition while k_B is Boltzmann constant.

The autoignition temperature of ethanol is affected by the sensor material that works as a catalyst for the reaction of ethanol with the oxygen in the atmosphere. The concentration of the burning gas can be represented by a logistic function (Abdulsattar, 2023a):

$$f(T) = \frac{1}{1 + e^{k_s(T-T_0)}} \tag{3}$$

In the above equation, k_s is related to the steepness of ethanol concentration decrease while T_0 is the temperature at which the ethanol concentration reaches half of its original concentration.

The Gibbs free of transition ($\Delta G^{\ddagger}$) can be evaluated using the (ts) transition state option of transition state evaluation in the Gaussian 09 program. The transition state of ethanol is evaluated for the pristine SnO_2 and Mo-doped SnO_2 as in Fig. 1. At Mo-doped SnO_2 in small percentages (or high percentages) that cannot be evaluated directly, the modified Evans–Polanyi principle is used by interpolation (or extrapolation for high percentages) (Abdulsattar, 2023b):

$$\Delta G^{\ddagger} = \Delta G_0^{\ddagger} + \beta \Delta G_1^{\ddagger} \tag{4}$$

In the above equation, $\Delta G_0^{\ddagger}$ and β are parameters that fit the Gibbs transition state energy line for pristine and Mo-doped SnO2.

The experimental response is defined (for reducing gases) as the ratio of the resistance in the air (Ra) to the resistance when the ethanol vapor exists in the air (Rg), i.e. (Ra/Rg). The theoretical response is correlated linearly to the reaction rate (Eq. (1)) by the equation (Abdulsattar and Mahmood, 2023):

$$\text{Response(theoretical)} = 1 + C\left|\frac{d[SnO_2]}{dt}\right| \tag{5}$$

3. Results and discussion results

Fig. 2 shows the variation of Gibbs energy of transition with temperature for the pristine and Mo-doped SnO2 clusters. As the doping molar percentage increases, the Gibbs energy increases. This behavior is the opposite of what happens when doping with Pt group or noble metals (Abdulsattar et al., 2024). However, the response increases in both cases of doping, as will be explained later.

Fig. 3 shows the variation of theoretical response for pristine and Mo-doped SnO2 (0, 3, 5, 7% molar ratio) with temperature compared with experimental results (Ra/Rg) (Wang et al., 2021) for 100 ppm C2H6O. The highest response is for 5% Mo-doped SnO2 at 220 °C for the Mo-doped SnO2 while the pristine SnO2 is at 240 °C. In all Fig. 3 results, the response increases as temperature increases. However, as the temperature reaches 220 °C for the doped SnO2, another reaction channel takes place, namely the reaction of ethanol with atmospheric oxygen and not with the sensor material. The concentration of ethanol decreases rapidly, and as a result, the reaction rate of ethanol with the sensor material decreases as in Eq. (1). The autoignition temperature of ethanol at 368 °C is reduced to nearly 240 °C for pristine SnO2 and 220 °C for Mo-doped SnO2. This shows that doping not only increases the response value but also decreases the highest response temperature. As doping percentage increases, the lattice distortion increases as can be seen in Fig. 1 that increases the resistance of the lattice. However, as doping passes 5% a new MoO3 phase begins to form that reduces the overall resistance of the lattice. This is confirmed by the values of the C parameter in Table 1 below.

Fig. 4 shows the variation of theoretical response for pristine and Mo-doped SnO2 (5% molar ratio) with C2H6O concentration at 220 °C temperature compared with experimental results. The variation of response with ethanol concentration is linear or nearly linear in the pristine SnO2 case due to the abundance of reaction sites. The variation of response with ethanol concentration is parabolic due to the limited reaction sites in the Mo-doped SnO2 case (only 5% sites (Mo-doped) are responsible for the high response values).

Fig. 5 shows ethanol experimental (Wang et al., 2021) and theoretical response time for the pristine and 5% Mo-doped SnO2 sensor as a function of temperature. The response time has a minimum value of 240 or 220 °C for pristine and 5% Mo-doped SnO2. The response time is calculated by integrating the 90% response time:

$$t_{res(90\%)} = \frac{In(10)}{[C_2H_6O]_e^V A T^m \, exp\left(\frac{-\Delta G^{\ddagger}}{K_B T}\right)} \tag{6}$$

The response time is defined as the time needed to reach 90% of equilibrium resistance.

Fig. 6 shows the effect of relative humidity on the theoretical and experimental response for 50 ppm C2H6O at 220 °C for the 5% Mo-doped sensor. The complete burning of ethanol as it reacts with the Mo-doped SnO2 sensor cluster can be given by the equation:

$$6MoSn9O17 + C2H6O \rightarrow 6MoSn9O16 + 2CO2 + 3H2O \tag{7}$$

As can be seen from the above equation, H2O is one of the products of ethanol burning. The equilibrium constant is defined in terms of forward and backward reaction concentrations. As the humidity

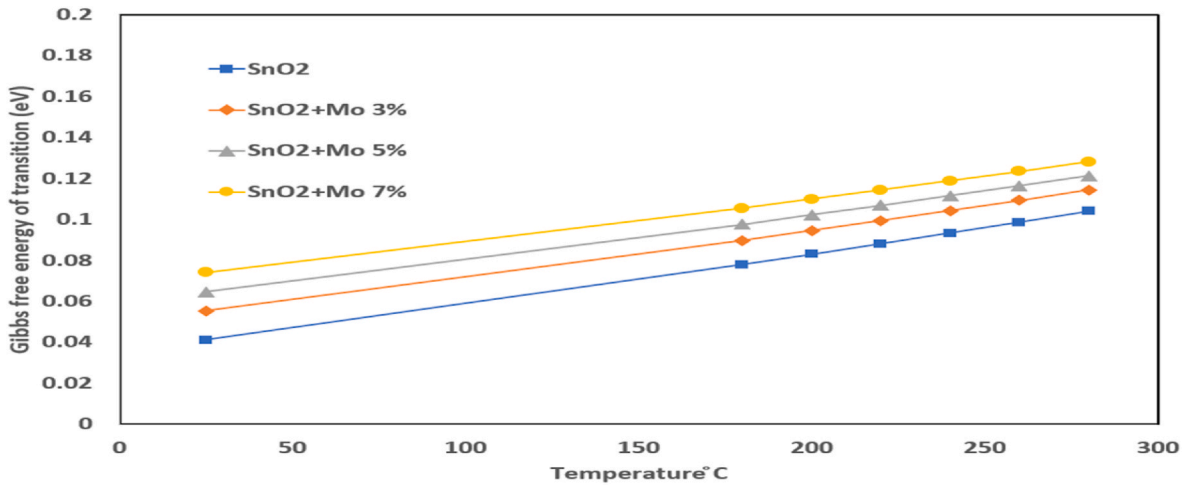

Fig. 2. Gibbs free energy of transition of pristine and 3, 5, 7% (molar) Mo-doped SnO_2 clusters as a function of temperature.

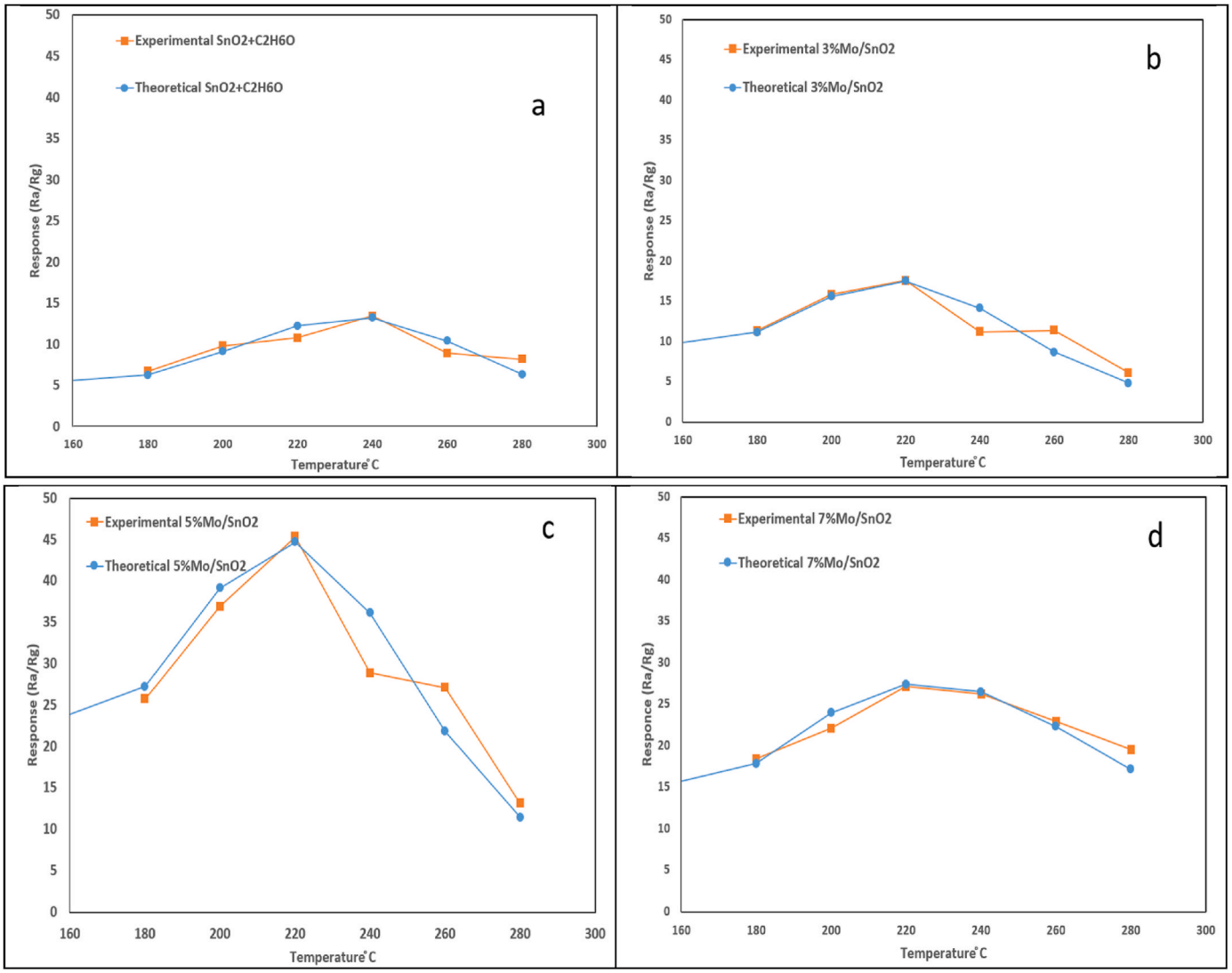

Fig. 3. The variation of theoretical response for pristine and Mo-doped SnO_2 (3, 5, 7% molar ratio) with temperature compared with experimental results (Ra/Rg) (Wang et al., 2021) for 100 ppm C_2H_6O.

Table 1
Parameters used to simulate C_2H_6O gas sensing reaction model of pristine and different Mo-doped SnO_2. $\Delta G^{\ddagger}$ values are at 25 °C temperature and normal pressure.

No.	Reaction	$\Delta G^{\ddagger}$ (eV)	A	m	v	k_s (K^{-1})	T_0 (°C)	C (s)
1	$[SnO_2\cdots C_2H_6O]^a \downarrow [SnO_2\cdots C_2H_6O]^{\ddagger}$	0.0412	$3.67\ 10^{-29}\ s^{-1}.\ K^{-12}$	12	1	0.06	245	144
2	$[3\%Mo/SnO_2\cdots C_2H_6O]^a \downarrow [3\%Mo/SnO_2\cdots C_2H_6O]^{\ddagger}$	0.0553	$9.00\ 10^{-31}\ s^{-1}.\ K^{-12}$	12	½	0.06	225	160
3	$[5\%Mo/SnO_2\cdots C_2H_6O]^a \downarrow [5\%Mo/SnO_2\cdots C_2H_6O]^{\ddagger}$	0.0647	$3.50\ 10^{-30}\ s^{-1}.\ K^{-12}$	12	½	0.06	225	130
4	$[7\%Mo/SnO_2\cdots C_2H_6O]^a \downarrow [7\%Mo/SnO_2\cdots C_2H_6O]^{\ddagger}$	0.0741	$5.10\ 10^{-30}\ s^{-1}.\ K^{-12}$	12	½	0.04	215	82

increases, an increase in H2O concentration occurs, which increases the backward reaction and leads to a decrease in the overall reaction. In addition to the backward reaction, the water molecules that form on the sensor surface serve as a barrier that prevents further ethanol-forward reactions. As a result, the constant A in Eq. (1) decreases as the humidity increases. Practically, the following equation relates the A constant with humidity that describes the theoretical response of Fig. 6:

$$A = (3.5–0.022\ RH\%)\ 10–31 \quad (8)$$

Fig. 7 shows the theoretical HOMO (highest occupied molecular orbital) and LUMO (lowest unoccupied molecular orbital) and energy gaps of SnO2 and Mo/SnO2 that correspond to the two figures Fig. 1a and b. The experimental energy gap of pristine SnO2 is 3.6–3.8 eV (Parida and Bhowmik, 2023) compared to the present calculated 3.867 eV. Fig. 7 shows that the energy gap did not change appreciably despite Mo-doping. The unchanged energy gap is because MoO3 is a high energy gap semiconductor with an energy gap larger than 3 eV (V.K. et al., 2024) which is very close to that of SnO2. However, HOMO and LUMO rises slightly for the Mo/SnO2 case.

Table 1 shows the parameters used in the theoretical simulation of

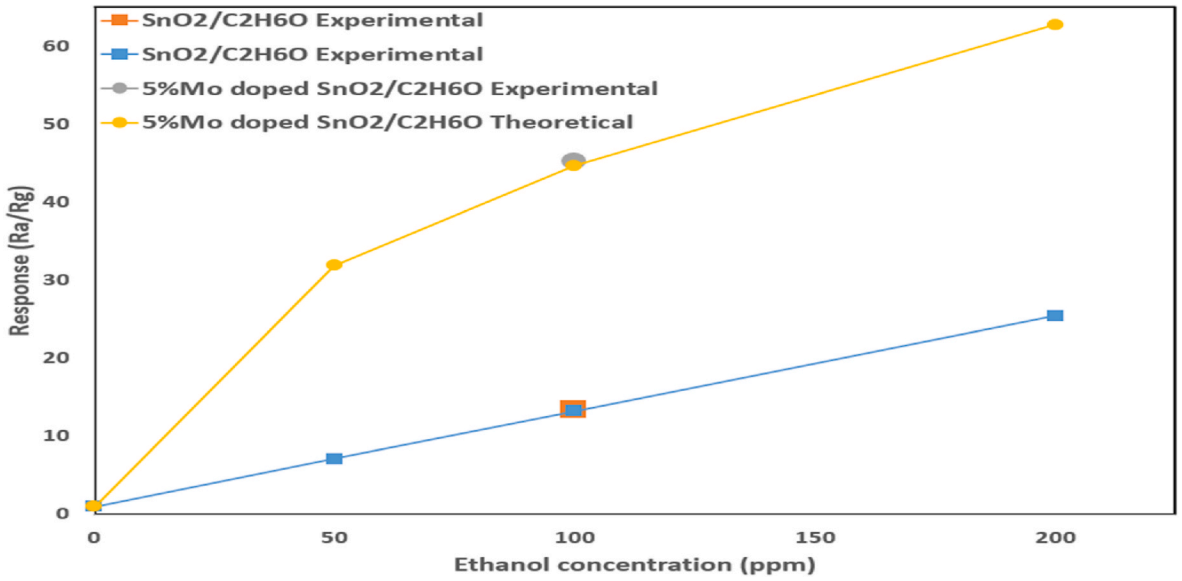

Fig. 4. The variation of theoretical response for pristine and Mo-doped SnO_2 (5% molar ratio) with C_2H_6O concentration at 220 °C temperature compared with experimental results (Ra/Rg).

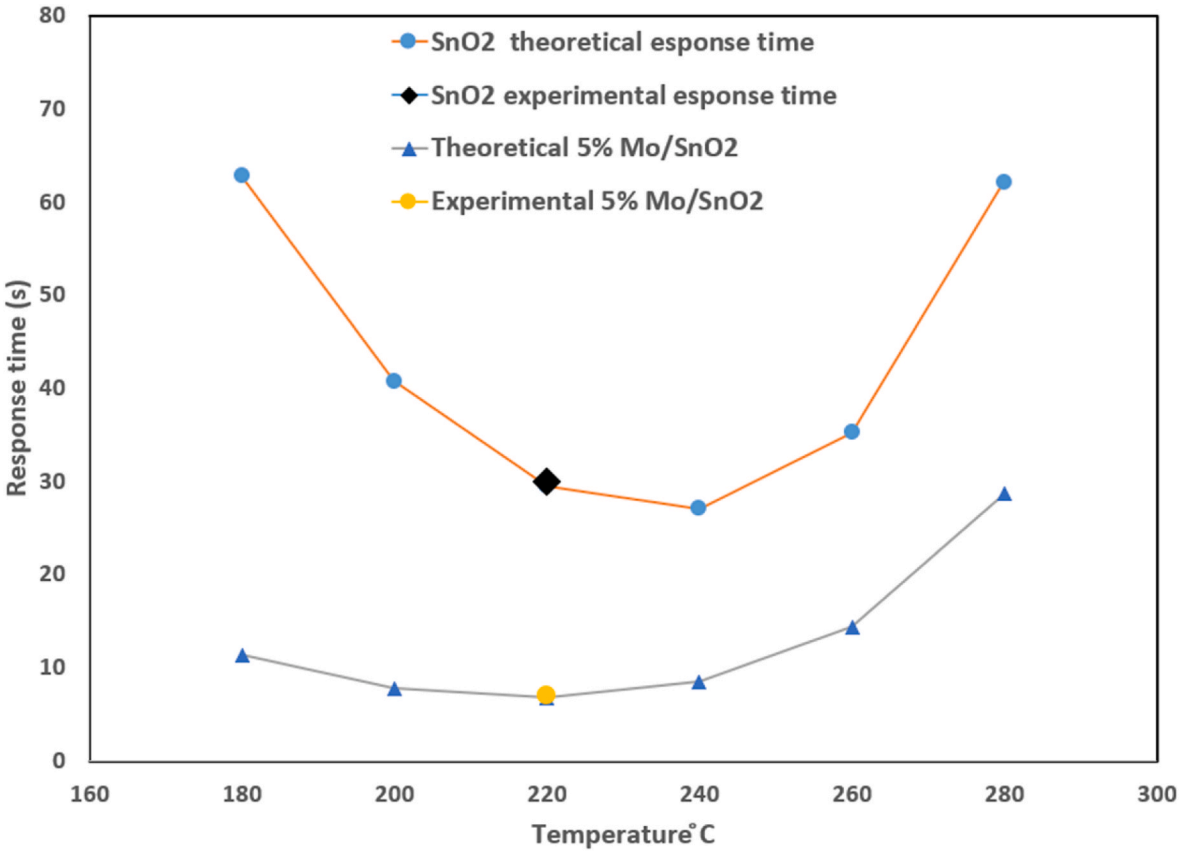

Fig. 5. Experimental (Wang et al., 2021) and theoretical response time for the pristine and 5% Mo-doped SnO_2 sensor as a function of temperature for ethanol.

response and response time for the pristine and different Mo-doping percentages of SnO2. In all reactions of Table 1, an adsorption state is formed first, followed by a transition state. For example, the reaction no. 1 for the pristine SnO2 reaction with C2H6O, an adsorption state labeled [SnO2···C2H6O]a is formed first. The adsorption of ethanol on the pristine and Mo-doped SnO2 clusters surface of Fig. 1a and b are −0.573 and −0.713 eV, respectively. These values show stronger adsorption after doping due to higher charges on Mo-doping sites, as can be proved using NBO (Natural Bond Orbitals) calculation. After the formation of the adsorption state, the ethanol molecule tries to react with the SnO2 cluster by crossing a potential barrier of the transition state labeled [SnO2···C2H6O]‡. The values of the difference in Gibbs energy for these two states are called the Gibbs free energy of transition (ΔG‡) as in Eq. (1). The values of ΔG‡ in Table 1 show increasing order as the doping

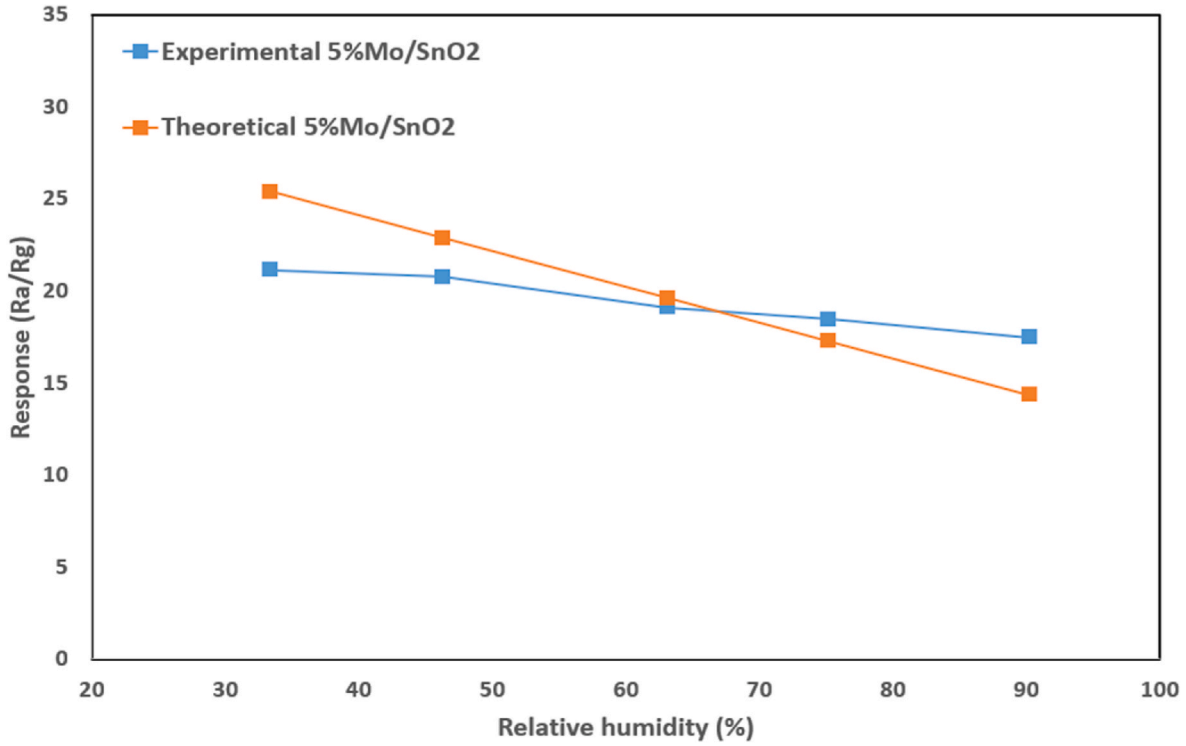

Fig. 6. Effect of relative humidity on the theoretical and experimental response for 50 ppm C_2H_6O at 220 °C for the 5% Mo-doped sensor.

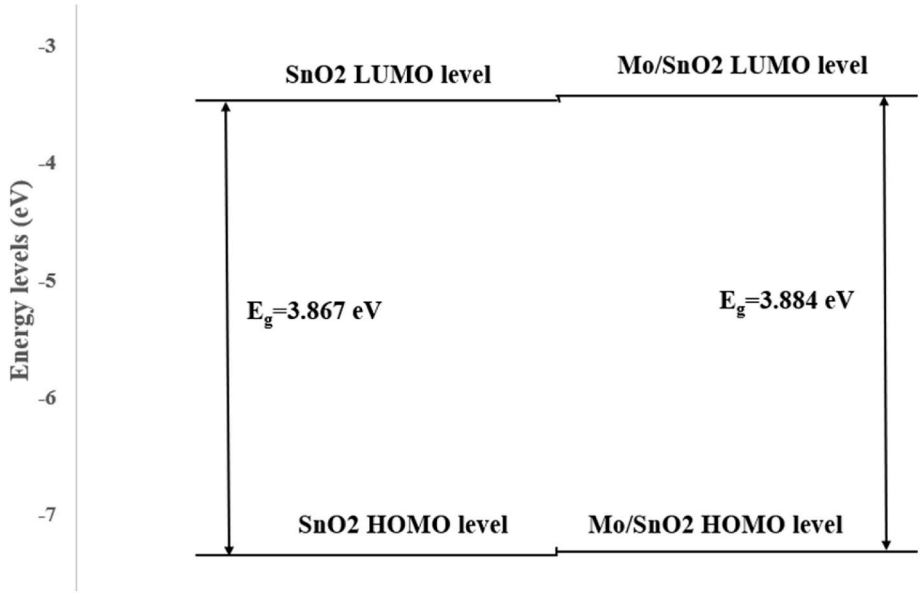

Fig. 7. Theoretical HOMO and LUMO and energy gap of SnO_2 and Mo/SnO_2 that corresponds to the two figures, Fig. 1a and b.

increases. This is the reverse order when doping with a platinum group or noble elements (Abdulsattar et al., 2024). The reason for this contradiction is the difference in chemical activity between these two types of elements. However, the response of the two kinds of doping increases for two reasons, as discussed later. Temperature dependence of Gibbs free energy of adsorption or transition is directly related to the change in entropy as in the equation (Abdulsattar et al., 2024):

$$\Delta G^{\ddagger} = \Delta H^{\ddagger} - T\Delta S^{\ddagger} \quad (4)$$

In the above equation $\Delta H^{\ddagger}$ is the enthalpy of transition, while $\Delta S^{\ddagger}$ is the entropy of transition that increases upon doping.

Parameter A in Table 1 represents the structural effects of the reaction between the sensor and the gas, as in Eq. (1). Parameter A increases with the increase of doping. However, this increase in A is confronted by a decrease in the C parameter, representing the effect of the variation in resistivity due to doping. The net result of the two variations is that the 5% Mo-doped SnO_2 has the highest response of all samples. The Mo-doped SnO_2 sensor has also proved to have good stability for at least 90 days after manufacturing, which means that the constant A does not change with time appreciably (Wang et al., 2021).

The m parameter in Table 1 also appears as the temperature exponent in Eq. (2). The high value of this parameter is due to the reaction,

structural, and diffusion effects of the detected gas and the sensor material surface effects (Abdulsattar et al., 2024). The other exponent parameter is the v parameter, which appears as the ethanol gas concentration parameter. This parameter has the value 1 for the pristine and ½ for the doped SnO_2 cluster. The cause of this difference is that abundant reaction sites on the pristine SnO_2 surface cause the response to behave linearly with gas concentration (exponent equal to 1). In contrast, fast-depleting reaction sites (3% of all sites in 3% Mo-doped SnO_2) cause the response proportional to the gas concentration to the power ½.

The remaining two parameters describe the autoignition of ethanol as the temperature approaches the autoignition temperature at 368 °C. The pristine SnO_2 sensor acts as a catalyst to decrease the autoignition temperature near 245 °C. However, 3% and 5% Mo-doped SnO_2 decreases the autoignition to 225 and 215 °C for the 7% Mo-doped SnO_2. This shows the increasing effect of doping that reduces the autoignition temperature. The k_s parameter that describes the steepness of the decrease of ethanol concentration is nearly constant and decreases as the doping concentration reaches 7% Mo-doped SnO_2.

4. Conclusions

The response and response time of pristine and Mo-doped SnO_2 pyramid clusters towards ethanol are compared to available experimental data. The effect of humidity is considered and compared well with experimental data. The novelty of the present work is that it considers the impact of ethanol properties into account when calculating the response of pristine and Mo-doped SnO_2 pyramid clusters. The autoignition temperature of ethanol is considered by using a logistic function. The transition state theory calculates the response by evaluating Gibbs free energy of transition. Modified Evans–Polanyi principle calculates Gibbs free energy of transition for the different Mo-doping percentages. Unlike doping with a platinum group or noble elements, the Gibbs energy of transition increases with increased Mo-doping percentages. However, other model parameters increase the response due to structural, diffusion, and surface area effects. Mo-doped SnO_2 shows high response, short response time, and stability towards ethanol that nominate the sensor for practical applications.

CRediT authorship contribution statement

Mudar Ahmed Abdulsattar: Writing – review & editing, Writing – original draft, Project administration, Formal analysis, Data curation, Conceptualization. **Rashid Hashim Jabbar:** Methodology, Investigation. **Mohammed A. Al-Seady:** Visualization, Validation.

Declaration of competing interest

The authors declare that they have no known competing financial interests or personal relationships that could have appeared to influence the work reported in this paper.

Data availability

Data will be made available on request.

References

Abdulsattar, M.A., 2020. Transition state theory application to H2 gas sensitivity of pristine and Pd doped SnO2 clusters. Karbala International Journal of Modern Science 6, 13. https://doi.org/10.33640/2405-609X.1615.

Abdulsattar, M.A., 2023a. GaxIn2-xO3 surface pyramids interaction with formaldehyde: thermodynamic and sensing analysis. Karbala International Journal of Modern Science 9, 8. https://doi.org/10.33640/2405-609X.3324.

Abdulsattar, M.A., 2023b. The reaction of pristine and Rh-doped SnO2 clusters with acetone: application of Evans–Polanyi principle to transition state theory. J. Mol. Model. 29 https://doi.org/10.1007/s00894-023-05710-5.

Abdulsattar, M.A., Mahmood, T.H., 2023. Enhancement of SnO2 sensitivity to acetone by Au loading: an application of Evans–Polanyi principle in gas sensing. Optik 275, 170604. https://doi.org/10.1016/j.ijleo.2023.170604.

Abdulsattar, M.A., Abduljalil, H.M., Abed, H.H., Al-Seady, M.A., 2024. Temperature and humidity effects on the acetone gas sensing of pristine and Pd-doped WO3 clusters: a transition state theory study. J. Mol. Model. 30 https://doi.org/10.1007/s00894-024-06016-w.

Afifah, N., Sarifudin, A., Purwanto, W.W., Krisanti, E.A., Mulia, K., 2024. Glucomannan isolation from porang (Amorphophallus muelleri Blume) flour using natural deep eutectic solvents and ethanol: a comparative study. Food Chem. 453 https://doi.org/10.1016/j.foodchem.2024.139610.

Araújo, E.P.d., Paiva, M.P., Moisés, L.A., Santo, G.S.d.E., Blanco, K.C., Chiquito, A.J., Amorim, C.A., 2023. Improving hazardous gas detection behavior with palladium decorated SnO2 nanobelts networks. Sensors 23. https://doi.org/10.3390/s23104783.

Bonyani, M., Zebarjad, S.M., Mirzaei, A., Kim, T.U., Kim, H.W., Kim, S.S., 2024. Electrospun ZnO hollow nanofibers gas sensors: an overview. J. Alloys Compd. 1001. https://doi.org/10.1016/j.jallcom.2024.175201.

Chen, C.-C., Liaw, H.-J., Shu, C.-M., Hsieh, Y.-C., 2010. Autoignition temperature data for methanol, ethanol, propanol, 2-butanol, 1-butanol, and 2-methyl-2,4-pentanediol. J. Chem. Eng. Data 55, 5059–5064. https://doi.org/10.1021/je100619p.

Chen, X., Liu, T., Wu, R., Yu, J., Yin, X., 2022. Gas sensors based on Pd-decorated and Sb-doped SnO2 for hydrogen detection. J. Ind. Eng. Chem. 115, 491–499. https://doi.org/10.1016/j.jiec.2022.08.035.

Chen, M., Chang, K., Zhang, Y., Zhang, Z., Dong, Y., Qiu, X., Jiang, H., Zhu, Y., Zhu, J., 2023. Cation-radius-controlled Sn−O Bond length boosting CO2 electroreduction over Sn-based perovskite oxides. Angewandte Chemie - International Edition 62. https://doi.org/10.1002/anie.202305530.

Ding, Y., Du, B., Guo, X., Dong, Y., Zhang, M., Jin, W., Gao, C., Peng, D., He, Y., 2024. An ultrasensitive NO2 gas sensor based on a NiO-SnO2 composite with a sub-ppb detection limit at room temperature. Sensor. Actuator. B Chem. 414 https://doi.org/10.1016/j.snb.2024.135916.

He, W., Zhao, Z., Zhang, Z., Xiao, F., 2024. Modification and application of the Arrhenius equation based on activated energy methods from various asphalt binders. J. Mater. Civ. Eng. 36 https://doi.org/10.1061/jmcee7.mteng-17482.

Hsu, K.C., Fang, T.H., Hsiao, Y.J., Chan, C.A., 2020. Highly response CO2 gas sensor based on Au-La2O3 doped SnO2 nanofibers. Mater. Lett. 261. https://doi.org/10.1016/j.matlet.2019.127144.

Hydrogen autoignition temperature, (n.d.). https://www.wolframalpha.com/input/?i=hydrogen+autoignition+temperature (accessed December 23, 2023).

Jagadish, K., Rai, R.K., Pandey, M., Chandni, U., Ravishankar, N., 2022. Mutual stabilization of metastable phases of tin oxide: epitaxial encapsulation of tetragonal SnO microcrystals by orthorhombic SnO2. J. Phys. Chem. C. https://doi.org/10.1021/acs.jpcc.2c03729.

Knopf, D.A., Ammann, M., 2021. Technical note: adsorption and desorption equilibria from statistical thermodynamics and rates from transition state theory. Atmos. Chem. Phys. 21, 15725–15753. https://doi.org/10.5194/acp-21-15725-2021.

Mafa, P.J., Malefane, M.E., Opoku, F., Sacko, A., Oladipo, A.O., Lebelo, S.L., Liu, D., Gui, J., Mamba, B.B., Kuvarega, A.T., 2023. Experimental and theoretical confirmation of CeFeCu trimetal oxide/Bi2O3 S-scheme heterojunction for boosted photocatalytic degradation of sulfamethoxazole and toxicity evaluation. J. Clean. Prod. 429 https://doi.org/10.1016/j.jclepro.2023.139519.

Malefane, M.E., Feleni, U., Mafa, P.J., Kuvarega, A.T., 2020. Fabrication of direct Z-scheme Co3O4/BiOI for ibuprofen and trimethoprim degradation under visible light irradiation. Appl. Surf. Sci. 514 https://doi.org/10.1016/j.apsusc.2020.145940.

Manikandan, V., Petrila, I., Vigneselvan, S., Mane, R.S., Vasile, B., Dharmavarapu, R., Lundgaard, S., Juodkazis, S., Chandrasekaran, J., 2020. A reliable chemiresistive sensor of nickel-doped tin oxide (Ni-SnO2) for sensing carbon dioxide gas and humidity. RSC Adv. 10, 3796–3804. https://doi.org/10.1039/c9ra09579a.

Material Safety Data Sheet (Acetone MSDS), (n.d.). https://www.collectioncare.org/MSDS/Acetonemsds.pdf (accessed October 3, 2022).

Nguyet, T.T., Hung, C.M., Hong, H.S., Thai, N.X., Thang, P.V., Thi Xuan, C., Van Duy, N., Thi Theu, L., Van An, D., Nguyen, H., Ou, J.Z., Chien, N.D., Hoa, N.D., 2024. Enhanced response characteristics of NO2 gas sensor based on ultrathin SnS2 nanoplates: experimental and DFT study. Sensor Actuator Phys. 373 https://doi.org/10.1016/j.sna.2024.115384.

Nzaba, S.K.M., Mmelesi, O.K., Malefane, M.E., Mafa, P.J., Mamba, B.B., Kuvarega, A.T., 2024. Comparative study of visible-light active BiOI and N,Pd-TiO2 photocatalysts: catalytic ozonation for dye degradation. Colloids Surf. A Physicochem. Eng. Asp. 684. https://doi.org/10.1016/j.colsurfa.2024.133167.

Pan, Z., Wang, D., Zhang, D., Yang, Y., Yu, H., Wang, T., Dong, X., 2024. rGO doped MOFs derived α-Fe2O3 nanomaterials for self-supporting ppb-level NO2 gas sensor. Sensor. Actuator. B Chem. 405 https://doi.org/10.1016/j.snb.2024.135378.

Parida, B.K., Bhowmik, R.N., 2023. Synthesis of Fe and La doped SnO2 system in ambient and non-ambient conditions: effect on lattice structure, chemical state, optical and dielectric properties. Ceram. Int. 49, 34582–34594. https://doi.org/10.1016/j.ceramint.2023.08.102.

Redd, M.E., Guffey, C.J., Gustafson, E.L., Hart, E.H., McQuade, K.S., Giles, N.F., Knotts IV, T.A., Wilding, W.V., 2024. Autoignition temperature trends for various chemical families. Fuel 355. https://doi.org/10.1016/j.fuel.2023.129321.

Sahu, B.K., Das, A., 2018. Significance of in-plane oxygen vacancy rich non-stoichiometric layer towards unusual high dielectric constant in nano-structured SnO2. Phys. E Low-dimens. Syst. Nanostruct. 103, 60–65. https://doi.org/10.1016/j.physe.2018.05.016.

Shefer, I., Lopez, K., Straub, A.P., Epsztein, R., 2022. Applying transition-state theory to explore transport and selectivity in salt-rejecting membranes: a critical review. Environ. Sci. Technol. 56, 7467–7483. https://doi.org/10.1021/acs.est.2c00912.

Thirumoorthi, M., Prakash, J.T.J., 2016. Effect of F doping on physical properties of (211) oriented SnO2 thin films prepared by jet nebulizer spray pyrolysis technique. Superlattice. Microst. 89, 378–389. https://doi.org/10.1016/j.spmi.2015.11.023.

Vaishampayan, M.V., Deshmukh, R.G., Walke, P., Mulla, I.S., 2008. Fe-doped SnO2 nanomaterial: a low temperature hydrogen sulfide gas sensor. Mater. Chem. Phys. 109, 230–234. https://doi.org/10.1016/j.matchemphys.2007.11.024.

van Dyk, J., Görgens, J.F., van Rensburg, E., 2024. Enhanced ethanol production from paper sludge waste under high-solids conditions with industrial and cellulase-producing strains of Saccharomyces cerevisiae. Bioresour. Technol. 394 https://doi.org/10.1016/j.biortech.2023.130163.

V.K, E., H, R., H.S, B., P.M, S., D.S, S., K.S, B.E., G, A., G, N., 2024. Facile green synthesis of Zn doped MoO3 nanoparticles and its photocatalytic and photoluminescence studies. J. Mol. Struct. 1312. https://doi.org/10.1016/j.molstruc.2024.138494.

Wang, L., Ma, S., Li, J., Wu, A., Luo, D., Yang, T., Cao, P., Ma, N., Cai, Y., 2021. Mo-doped SnO2 nanotubes sensor with abundant oxygen vacancies for ethanol detection. Sensors and Actuators B: Chemical. 347 https://doi.org/10.1016/j.snb.2021.130642.

Xu, X., Liu, W., Jiang, H., Ma, W., Wang, M., Sun, G., 2024. Design of mesoporous Carbon/SnO2 micro/nanostructured ethanol sensors. Mater. Sci. Semicond. Process. 179 https://doi.org/10.1016/j.mssp.2024.108479.

Yang, B., Thi Hanh To, D., Sobolak, D., Mendoza, E.R., Myung, N.V., 2024. High performance methyl salicylate gas sensor based on noble metal (Au, Pt) decorated WO3 nanofibers. Sensor. Actuator. B Chem. 413 https://doi.org/10.1016/j.snb.2024.135741.

Zhu, X., Li, J., Chang, X., Gao, W., Chen, X., Niu, S., Sun, S., 2024. Room temperature gas sensors for NH3 detection based on SnO2 films and lamellar-structured Ti3C2Tx MXene heterojunction nanocomposites. Appl. Surf. Sci. 660 https://doi.org/10.1016/j.apsusc.2024.159976.